

Interpretation of x-ray emission spectra: NO adsorbed on Ru(001)

M. Staufer, U. Birkenheuer, T. Belling, F. Nörtemann, and N. Rösch^{a)}
Lehrstuhl für Theoretische Chemie, Technische Universität München, D-85747 Garching, Germany

M. Stichler, C. Keller, W. Wurth, and D. Menzel
Physik Department E20, Technische Universität München, D-85747 Garching, Germany

L. G. M. Pettersson
FYSIKUM, University of Stockholm, Box 6730, S-113 85 Stockholm, Sweden

A. Föhlisch and A. Nilsson
Department of Physics, Uppsala University, Box 530, S-751 21 Uppsala, Sweden

(Received 20 January 1999; accepted 16 June 1999)

A density functional investigation of the x-ray emission spectrum of NO adsorbed on Ru(001) has been carried out using model cluster calculations. The dipole matrix elements governing the emission probability were evaluated in the frozen ground-state approximation. The resulting simulated spectra exhibit all characteristic features of the experimental data. A detailed analysis of the electronic structure of the model clusters permits a complete rationalization of all observed trends. Furthermore, a picture of the surface chemical bond results in which the classical Blyholder frontier orbital model is extended to a three-orbital description for both the π and σ interactions. Comparison of different adsorption sites reveals that threefold coordinated NO features a stronger orbital interaction with the substrate than NO adsorbed in an on-top position. © 1999 American Institute of Physics. [S0021-9606(99)01434-8]

I. INTRODUCTION

While x-ray emission spectroscopy (XES) has been in use for free molecules and crystals quite a long time,¹⁻⁴ the availability of third-generation synchrotron light sources promoted the application of this technique to adsorbates on surfaces.⁵⁻⁹ The core hole creation process which precedes the actual x-ray emission allows the selective excitation of individual atoms of an adsorbate. This has been demonstrated recently even for the two atoms of a N₂ molecule adsorbed on Ni(001).^{10,11} If measured in angular resolved fashion, the emitted photons finally yield energy-, atom-, and symmetry-resolved information about the electronic structure of the systems under study. Thus, x-ray emission spectroscopy provides insight into adsorption systems at a level of detail which up to now had been reserved for quantum chemistry methods. In fact, XES can be employed as a kind of experimental population analysis, as will be demonstrated in this study, at least to the extent that the salient features found experimentally can be interpreted in a frozen orbital model as advocated here and by similar model calculations.¹¹⁻¹³ X-ray emission intensities are very sensitive to the character and shape of the electronic wave functions involved. Therefore, the correct determination of x-ray emission spectra by means of electronic structure calculations is quite a challenge to quantum chemistry methods. Yet, it has been demonstrated¹¹⁻¹⁶ and will be confirmed by the present work that electronic structure calculations are capable of revealing such subtle details. Thus, they are well suited for a detailed interpretation of XES data which goes far beyond the well-

established description of adsorption properties such as binding energies, adsorption geometries, or vibrational frequencies which, in a certain sense, only provide an averaged view of an adsorption system. In fact, by a careful analysis of the one-particle wave functions which result from conventional quantum chemistry or density functional calculations, deep insight into the surface chemical bond can be achieved; similar insight is now, in principle, also accessible via experiment.

Actually, x-ray emission from a strongly coupled adsorbate corresponds to a transition from a fully charge transfer-screened adsorbate core hole state to an equally fully screened adsorbate valence hole state. Calculations which take full account of all these relaxation processes are not yet feasible. In previous studies^{11-14,16} various one-particle approximations were applied. The frozen ground-state orbital approach, though certainly a strong approximation, was found to lead to the best agreement with symmetry-resolved experimental spectra. In any case, this frozen ground-state model is closer to reality than any model that takes into account relaxation phenomena on either the initial or the final state alone. We therefore used this approach here as well, and arrived, as will be shown, at the same overall positive conclusion.

The adsorption system NO/Ru(001) has recently been reinvestigated experimentally using x-ray emission spectroscopy.¹⁷ Stimulated by these measurements, a detailed analysis of the electronic structure of this adsorption system has been performed with special emphasis on the simulation of the x-ray emission intensities as a function of adsorption site and of the initial core hole state. The simulated spectra are first discussed at the effective one-particle

^{a)}Electronic mail: roesch@theochem.tu-muenchen.de

picture adopted for the calculation. Then, it will be demonstrated that most of the features of the experimental XES data are indeed very nicely reproduced by the frozen ground-state simulation. The adequacy of this one-particle approach to the interpretation of x-ray emission spectra will be discussed in more detail elsewhere.¹⁷ Here, we focus solely on the overall agreement that can be achieved by such a theoretical approach.

NO/Ru(001) has already been the subject of a combined experimental and theoretical study.¹⁸ That investigation was mainly dedicated to a rationalization of the vibrational spectra which had been recorded by means of high-resolution electron energy loss spectroscopy (HREELS) measurements.¹⁸ Below 200 K NO exists as a molecularly adsorbed species, either on top of substrate atoms or in threefold hollow sites.^{19,20} It was found¹⁸ that the two types of adsorption complexes exhibit quite different electronic structures which are manifested through a significantly lower NO stretching frequency for the threefold species (1400 cm^{-1}) compared to the on-top species (1800 cm^{-1}). In the case of the hollow site adsorption, this large vibrational frequency shift was rationalized by a negatively charged NO species. Yet, an analysis of the electronic structure of the adsorption complex was not the main issue of that work, especially because rationalizations in terms of one-particle orbitals may appear somewhat arbitrary or even a matter of taste without any direct comparison to experimental data. Now that x-ray emission data are available for NO/Ru(001) it is worthwhile to reinvestigate this adsorption system with special emphasis on the individual molecular orbitals (MOs) of the adsorption complexes.

A consistent picture of the surface chemical bond will arise from this analysis. Although NO and N₂ carry different numbers of electrons and different substrates are involved, the bonding mechanism of NO/Ru(001) will turn out to be quite similar to that found previously for N₂ and CO on Ni.^{11,21,22} This provides strong evidence for the general validity of the extended interaction scheme advocated here.

II. EXPERIMENTAL DETAILS

Since a detailed description of the experiments will be presented elsewhere,¹⁷ only a brief summary of the most important experimental aspects shall be given here. The experiments were carried out at Beamline 8.0 of the Advanced Light Source at Lawrence Berkeley National Laboratories, which is equipped with a modified spherical grating monochromator covering the energy region between 100 and 1300 eV. The high-level surface physics end station used at this beam line was constructed at the University of Uppsala; for a detailed description, see Refs. 23–25. It consists of a preparation chamber containing low-energy electron diffraction (LEED) optics, a mass spectrometer, and a gas doser system, and an analyzer chamber equipped with a Scienta SES-200 electron spectrometer,²⁶ an x-ray absorption detector,²⁷ and a grazing-incidence multiple-grating spectrometer^{28,29} for the detection of reflected and emitted soft x-ray photons.

For the procedures for sample and adlayer preparation and definition, see Ref. 17. Care was taken to exclude any degradation of the layers during data accumulation. For the

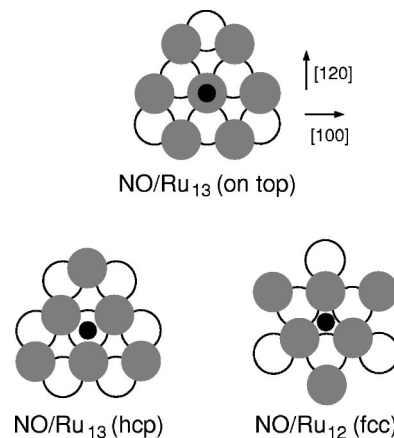


FIG. 1. Schematic representation of the cluster models. The substrate atoms are shown as gray (surface layer) and open (subsurface layer) circles. The position of the adsorbate is marked by the small black circle. NO is bound via the nitrogen center and with its molecular axis oriented normal to the surface.

measurement of the XES spectra, the sample was cooled to 80 K. The two NO species of interest were prepared separately in two different adsorption layers with oxygen as described in detail in Refs. 19 and 20. There is evidence that the presence of the coadsorbate does not significantly influence the XES spectra of the NO species.¹⁷

III. COMPUTATIONAL DETAILS

A. General

The calculations were performed with the program PARAGAUSS,^{30,31} a parallel implementation of the scalar relativistic linear combination of Gaussian-type orbitals density-functional (LCGTO-DF) method.^{32,33}

For ruthenium, a (17*s*,11*p*,8*d*) Gaussian orbital basis set^{34,35} was extended by one *s* exponent (0.2045), two *p* exponents (0.1634, 0.0635), and one *d* exponent (0.080 004). For nitrogen and oxygen, basis sets of the size (9*s*,5*p*,1*d*) were used³⁶ with the *d* exponents taken from Ref. 37. All basis sets were subject to generalized contractions³⁸ obtained from spin-restricted atomic calculations. The resulting contracted basis sets are [8*s*,6*p*,4*d*] for ruthenium and [5*s*,4*p*,1*d*] for oxygen and nitrogen. The local density functional in the form suggested by Vosko, Wilk, and Nusair,³⁹ together with the generalized gradient corrections (GGA) proposed by Perdew and Wang,⁴⁰ were applied throughout this study.

In accordance with experimental results,^{19,20} three different adsorption sites were considered. The corresponding model clusters are shown in Fig. 1. The geometry of the adsorption complexes was taken from a quantitative LEED analysis of the (2×2)-3NO/Ru(001) adsorption system where all three possible adsorption sites are realized.^{19,20} The surface layer relaxation and buckling found for this system was also included in the cluster models. However, to facilitate the computation, the slight deviation from the ideal C_{3v} symmetry configuration observed experimentally (lateral displacement of up to 0.08 Å) was not taken into account.

To simulate metallic behavior, fractional occupation numbers were adopted for the finite substrate model cluster in all of the calculations.³² To this end, the occupation numbers were chosen according to Fermi statistics by formally employing a temperature which corresponds to a kT value of 0.07 eV. The calculations were performed in spin-polarized fashion. Nevertheless, for all cluster models the spin difference turned out to be negligible once self-consistent field (SCF) convergence was reached.

B. XES spectra

Within the dipole approximation, the recombination of a valence orbital $|f\rangle$ and a previously generated core hole $|i\rangle$ is described by Fermi's golden rule

$$I(E) \propto (E_i - E_f)^4 \langle i | \mathbf{x} | f \rangle^2. \quad (1)$$

Following the strategy of recent successful simulations of the XES spectra of CO and N₂ adsorbed on Ni(100)^{11–13} the transition matrix element $\langle i | \mathbf{x} | f \rangle$ is evaluated in a one-particle approximation as a matrix element between appropriate Kohn–Sham orbitals which are taken from a ground-state calculation. Here, the $1s$ orbital of either the nitrogen or the oxygen center serves as the initial state, whereas for the final state the entire set of valence orbitals is considered.

It is experimentally well established that the initial state of the actual x-ray emission process is a fully relaxed core hole state.^{41,42} For a given XES spectrum it is the same for all emission processes. Core hole relaxation effects therefore do not affect the relative energies of the XES signals. Moreover, if the energy of the core hole state as measured by x-ray photoemission spectroscopy (XPS) is subtracted from the energies of the emitted XES photons, the resulting binding energies should equal the valence orbital ionization energies as measured by direct photoemission. It has also been demonstrated repeatedly that Kohn–Sham ground-state one-particle energies are well suited for providing a reasonable qualitative description of photoemission spectra.^{43–46} Hence, we adopt this procedure and identify the binding energies obtained in this way for the various valence orbitals with the corresponding Kohn–Sham one-particle energies.

Photoemission in the normal direction corresponds to an orientation of the polarization vector parallel to the surface. Assuming local C_{3v} symmetry of the adsorption complexes, only orbitals which belong to the twofold e representation are dipole active in this case. Grazing emission involves (in equal parts) polarization both perpendicular and parallel to the surface. By subtraction, a spectrum solely for polarization along the surface normal can be extracted.⁷ Only those orbitals which belong to the totally symmetric a_1 representation contribute to this spectrum. For convenience, the a_1 and e representations will be referred to as the σ and π representations of the $C_{\infty v}$ symmetry group of free NO in the following.

Since in the one-particle picture adopted here the transition intensity is determined by the matrix elements between a $1s$ orbital of nitrogen or oxygen and the valence orbitals, and since these $1s$ orbitals are strongly localized at the corresponding center and exhibit almost perfect spherical symmetry, the interpretation of XES spectra is rather simple. Only

TABLE I. Calculated properties of various NO/Ru(001) adsorption complexes: Mulliken charge q of the adsorbate NO and contributions q_σ and q_π from the σ and π interaction channels, dynamic dipole moment $\partial\mu/\partial z$ for the Ru–NO stretch mode, induced dipole moment $\Delta\mu$, and shift ΔE_F of the Fermi energy with respect to the bare substrate cluster (on-top: -4.03 eV, hcp and fcc: -4.01 eV).

Site	q (e)	q_σ (e)	q_π (e)	$\partial\mu/\partial z$ (e)	$\Delta\mu$ (e)	ΔE_F (eV)
on-top	-0.16	0.26	-0.42	0.27	0.14	0.07
hcp	-0.49	0.25	-0.74	-0.06	-0.76	-0.09
fcc	-0.36	0.25	-0.61	-0.10	-0.35	-0.16

final-state orbitals with local p -character around the nucleus in question are able to contribute to the transition matrix element. Using a linear combination of atomic orbitals (LCAO) description of the final-state orbitals, some p -character from each atomic basis function at the other adsorbate atoms will always exist at the specific $1s$ core site. However, because of the small spatial extent of the initial-state $1s$ orbital, these contributions will be of minor importance only and a one-center approximation is highly accurate. For that reason, XES spectra have sometimes been considered as an experimental analog to an atom-resolved orbital population analysis.^{3,11} On the other hand, one always has to keep in mind that the XES transition matrix elements are sensitive to the direct vicinity of the core region only. Thus, XES intensities of a specific $1s$ core hole do not fully reflect the overall character of a given final-state valence orbital.

To facilitate comparison with the experimental data, the calculated discrete spectra were subjected to a Gaussian broadening procedure (0.3 eV full width at half maximum).

IV. RESULTS AND DISCUSSION

A. General remarks

1. Adsorbate–substrate interaction

According to the Blyholder model,⁴⁷ bonding of a NO molecule to a transition metal species can be divided into σ donation and π back donation. The amount of electronic charge transferred from the adsorbate to the substrate and vice versa can roughly be estimated by a Mulliken population analysis (see Table I). σ electron charge donation from NO to the substrate is found to amount to about 0.25 e ; it is almost the same for all three adsorption sites. On the other hand, the amount of π back donation shows a significant site dependence. Compared to on-top adsorption, hollow site adsorption complexes feature a substantially stronger back donation, with the charge transfer at the hexagonal-close-packed (hcp) site being slightly higher than at the face-centered-cubic (fcc) site. As a consequence, at the hollow sites the adsorbate exhibits a significant negative net charge (see Table I) in accordance with previous assignments of the adsorbed species.¹⁸ At the on-top site, NO exists as an almost neutral species. To account for possible shortcomings of the Mulliken procedure, in the previous density functional (DF) study¹⁸ the substrate–adsorbate charge transfer was also investigated by means of static and dynamic dipole moments

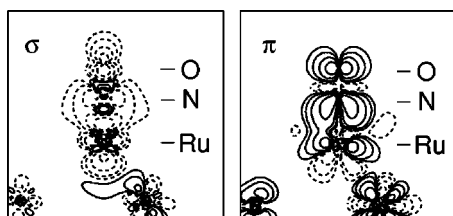


FIG. 2. Electron density difference between the model cluster Ru_{13}NO for on-top adsorption and its isolated constituents, Ru_{13} and NO , shown in the (100) plane. σ and π contributions are displayed separately. Solid lines represent electron accumulation, dashed lines electron depletion. The values of the contour lines are ± 0.032 , ± 0.010 , ± 0.0032 , and ± 0.0010 a.u. The positions of the various atoms are indicated by horizontal bars.

as well as by adsorbate-induced shifts of the Fermi energy of the model clusters. For comparison, the corresponding data obtained in the present GGA investigation are also given (Table I). They are in good agreement with the results reported previously,¹⁸ which were calculated in the $X\alpha$ approximation, corroborating these earlier local density approximation (LDA) results. There are several uncertainties related to the criteria employed to characterize the charge distribution, e.g., the influence of intraadsorbate and intra-substrate polarizations on the (dynamic) dipole moments or the effect of direct orbital interaction between adsorbate and substrate on the energy of the highest occupied orbital which serves as the Fermi level in a model cluster. Nevertheless, we are convinced that the overall qualitative picture derived from these criteria is correct: for hollow-site adsorption, a negatively charged NO species is found, whereas at the on-top site, the NO fragment carries noticeably less electronic charge and exists as an essentially neutral species on $\text{Ru}(001)$.

Previously, it has been argued^{19,48} that the different net charges of on-top and hollow-site NO species⁴⁹ are caused by an inverse Blyholder scheme in the π channel for the on-top species, i.e., electrons are transferred from the adsorbate to the substrate. However, examination of the adsorption-induced charge rearrangement by means of electron density difference plots (Fig. 2) reveals that this model does not hold for NO on $\text{Ru}(001)$. Obviously, in the σ channel the electron density of the adsorbate decreases significantly, whereas in the π channel electron accumulation around the nitrogen and oxygen centers is clearly discernible. Note that there exists no charge conservation within individual symmetry channels. According to the Blyholder model, back donation to the adsorbate should directly lead to a weakening of the NO π bond and to an elongation of the N–O distance. However, the LEED analysis^{19,20} yields a marginal shortening of the NO bond length for the on-top site by 0.02 Å compared to the gas phase. This can be regarded as a harbinger for necessary modifications to the classical Blyholder model of adsorbate–substrate bonding. The small decrease of electronic charge between the atoms of the adsorbate discernible in Fig. 2 provides further indication for a more complex bonding mechanism. We will return to this point in Sec. IV B 2.

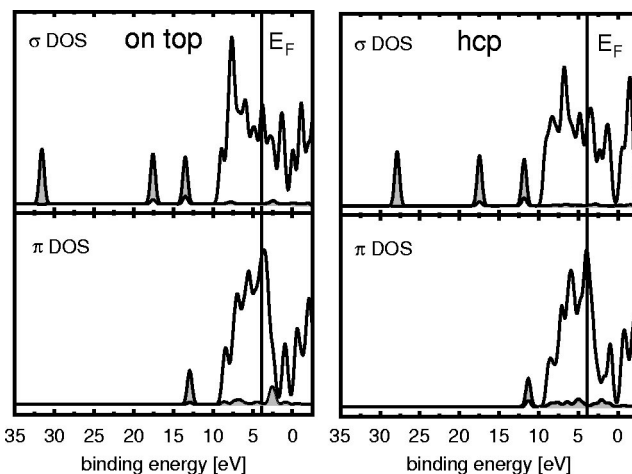


FIG. 3. Calculated density of states of the Ru_{13}NO cluster models for on-top (left panel) and hcp (right panel) adsorption, separated into σ and π interaction channels and projected onto adsorbate (shaded gray) and substrate. The projection is based on a Mulliken population analysis. The line spectra have been broadened by a Gaussian (half width 0.3 eV).

2. Density of states (DOS)

In Fig. 3, the densities of states of the on-top and the hcp model clusters are displayed. The metal sd band starts at binding energies of about 10 eV and extends to about 4 eV above the Fermi level. Three NO-dominated peaks can be seen in the σ channel; they derive from the 3σ , 4σ , and 5σ orbitals of NO. Since they are well separated from the metal band energetically, they are strongly adsorbate dominated. In the π channel, two different features are discernible below the Fermi level, a single isolated NO dominated peak well below the metal band at about 13 eV, and a broad manifold of states within the metal band with rather small NO contributions. The former peak derives from the adsorbate 1π orbital, whereas the latter feature is commonly referred to as the π resonance, associated with back donation; these levels arise from metal-dominated states. NO related peaks above the Fermi level also exist in the DOS of the σ and the π channel. Altogether, the DOS for the two adsorption sites look very similar. The main difference in the present context is that in the case of hollow-site adsorption, the metal contribution to the 1π state is larger and that, in turn, the NO π contributions to the back bonding orbitals are more pronounced.

B. Interpretation of the XES intensities

1. The σ channel

Like the DOS plots discussed before, the calculated XES spectra for the σ channel (Fig. 4) exhibit three major signals below 10 eV and one small signal at about 7.5 eV; they will be denoted as $3\tilde{\sigma}$ to $6\tilde{\sigma}$, respectively. Inspection of the electronic structure of the model clusters reveals that the $3\tilde{\sigma}$, the $4\tilde{\sigma}$, and the $5\tilde{\sigma}$ signals can actually each be assigned to *single* cluster orbitals. Some of these orbitals of the adsorption complex turn out to be quite different from those of the unperturbed reference molecular NO orbitals 3σ to 5σ ; a different designation is therefore helpful.

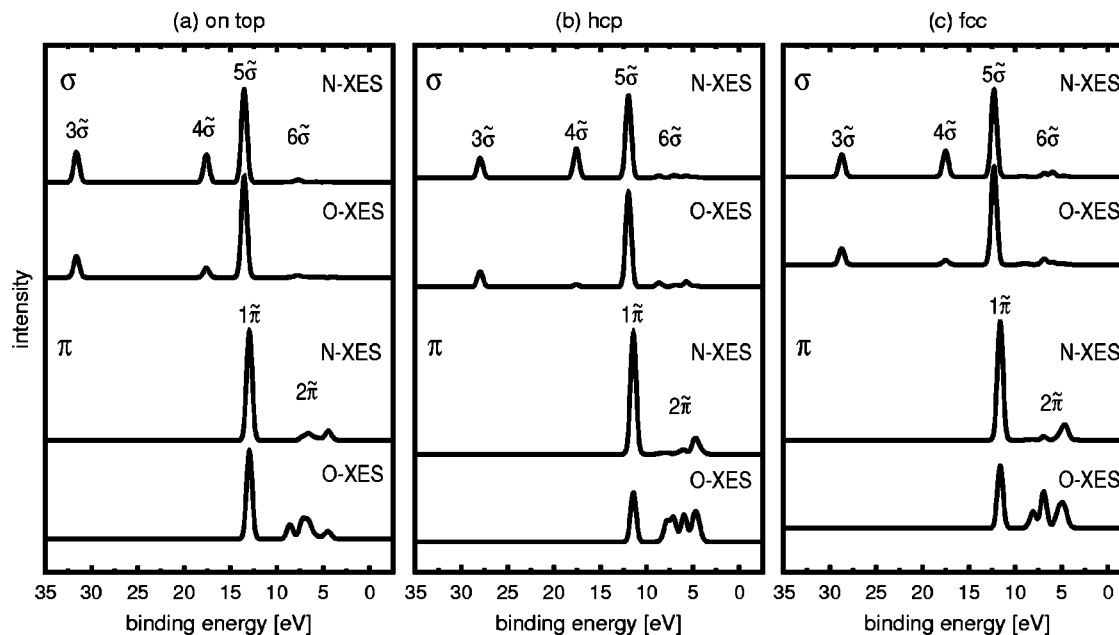


FIG. 4. Calculated N-edge and O-edge XES spectra of three model clusters for σ and π channels: (a) on-top adsorption complex Ru_{13}NO , (b) hcp adsorption complex Ru_{13}NO , (c) fcc adsorption complex Ru_{12}NO . The line spectra have been broadened by a Gaussian (half width 0.3 eV). The spectra for both types of core holes and all three adsorption sites are normalized to the same overall (σ plus π channel) intensity.

a. Analysis of the orbitals. A fragment orbital analysis has been used for examining the formation and shape of new orbitals within an adsorption complex. To this end, the molecular orbitals of the clusters are expressed as linear combinations of the molecular orbitals of the bare substrate clusters and the NO molecule (both in the geometry of the corresponding adsorption complex), and a Mulliken population analysis is applied to this decomposition.

This fragment analysis (Table II) reveals that the molecular NO 3σ orbital does not interact with any other orbital and thus entirely keeps its molecular character. In contrast, the 4σ and 5σ orbitals of NO strongly rehybridize upon interaction with the substrate. The final shape of these hybrid orbitals will provide the key to analyzing the relative intensities of the observed XES signal. As evident from Fig. 6 and Table III, the NO 4σ molecular orbital does not exhibit any nitrogen p contribution. Since only atomic p populations

contribute to the transition matrix elements, the intensity of the $4\tilde{\sigma}$ and $5\tilde{\sigma}$ signals in the N-edge spectra will thus exclusively depend on the amount of 5σ admixtures to the cluster orbitals $4\tilde{\sigma}$ and $5\tilde{\sigma}$. These admixtures are found to amount to roughly 20% and 60%, respectively, for all three adsorption sites investigated (Table II). The resulting ratio, 1:3, agrees very nicely with the observed relative intensities in the N-edge σ channel XES spectra (Fig. 4).

The major difference between the O- and the N-edge spectra is the remarkably low intensity of the $4\tilde{\sigma}$ signal in the O-XES spectra. This finding is due to the particular superposition of the NO 4σ and 5σ orbitals in the formation of the $4\tilde{\sigma}$ orbital of the adsorption complex. Both adsorbate MOs interact in a bonding fashion with the substrate. Thus, the 4σ and 5σ orbitals carry the same phase at the nitrogen site of the NO molecule, but opposite phases at the oxygen site (see Fig. 6). As a consequence, the oxygen p contributions of the two orbitals cancel each other to a large extent in the final $4\tilde{\sigma}$ cluster orbital. For the $5\tilde{\sigma}$ orbital of the adsorption complex, the phase relationship between the 5σ and 4σ MOs of NO is reversed. Therefore, constructive superposition of the p contributions results at the oxygen site which leads to the more pronounced $5\tilde{\sigma}$ feature in the O-edge spectra (see Fig. 4).

b. Site specific differences. The spectra for the fcc site resemble very much those calculated for the hcp site, indicating a rather similar adsorbate-substrate interaction at the two hollow sites. Thus, we will focus our discussion on the differences between the two hollow sites and the on-top site. The most significant distinction is the stronger reduction of the oxygen $4\tilde{\sigma}$ intensity for hollow-site adsorption. The fragment orbital analysis shows that the composition of the $4\tilde{\sigma}$ orbital in terms of NO MOs is almost identical for all sites.

TABLE II. Fragment orbital analysis of various adsorption model clusters for the cluster σ orbitals. Contributions of the NO reference orbitals (in percent) to the cluster orbitals. Contributions below 1% are not shown. Energies in eV.

Orbital	Site	Energy	Free NO contributions		
			3σ	4σ	5σ
$3\tilde{\sigma}$	top	31.59	101		
	hcp	27.86	99	1	
	fcc	28.62	100		
$4\tilde{\sigma}$	top	17.58		75	17
	hcp	17.47	1	74	17
	fcc	17.41	1	76	16
$5\tilde{\sigma}$	top	13.51		26	60
	hcp	11.84		26	59
	fcc	12.18		24	62

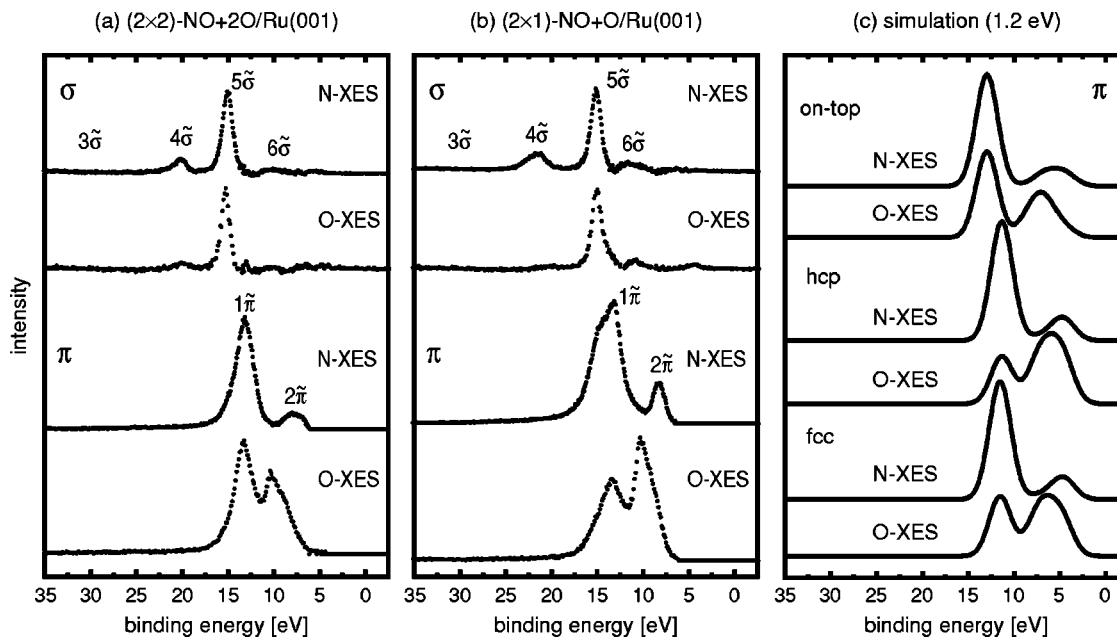


FIG. 5. Experimental N-edge and O-edge XES spectra for (a) (2×2) -NO+2O/Ru(001) (on-top) and (b) (2×1) -NO+O/Ru(001) (hollow site). The spectra for both types of core holes and the two adsorption sites are normalized to the same overall (σ plus π channel) intensity. The experimental binding energies are corrected by the respective work functions, 6.5 eV for (a) and 7.2 eV for (b). In (c), the π channel of the calculated N-edge and O-edge XES for all three model clusters is presented. A Gaussian broadening with a half width of 1.2 eV is applied to the theoretical raw data. The two peaks visible in every simulated spectrum represent the $1\tilde{\pi}$ and the $2\tilde{\pi}$ signals.

However, as a consequence of different values of the NO bond length, the shape of the free NO orbitals involved is site dependent. In the hcp site structure, the 4σ orbital of the noninteracting NO exhibits a lower O p population, whereas in the 5σ orbital the O p population is higher than in the NO orbitals in the on-top site geometry (see Table III). These slightly different compositions of the 4σ and 5σ molecular orbitals obviously lead to a more perfect cancellation of the O p contribution in the resulting $4\tilde{\sigma}$ cluster orbital in case of the hollow-site adsorption complex.

c. Comparison with the experimental spectra. Comparison between the experimental XES spectra and the calculated transition probability-weighted densities of states (Fig. 4) is complicated by the very large broadening of the $3\tilde{\sigma}$ and $4\tilde{\sigma}$ signals in the experimental spectra [Figs. 5(a), 5(b)]. In part, this broadening is caused by lifetime and many-body effects which are not included in the theoretical description adopted here. Apart from these missing effects in the $3\tilde{\sigma}$ signals, all qualitative characteristics of the experiment are reproduced by the simulated spectra. The calculated relative intensities of the $4\tilde{\sigma}$ and the $5\tilde{\sigma}$ orbitals show the same trend as in experiment. Also, the site dependence is predicted correctly by the simulations.

TABLE III. Atomic Mulliken p populations of the σ orbitals of a free NO molecule with the N–O distance as observed at the various adsorption sites.

Site	$d(\text{NO})$	3σ		4σ		5σ	
		O	N	O	N	O	N
on-top	1.13 Å	0.10	0.12	0.32	0.02	0.23	0.36
hcp	1.24 Å	0.08	0.10	0.23	0.01	0.32	0.37

2. The π channel

The π interaction of diatomics such as CO, N_2 , or NO with transition metal species is often reduced to an interaction of the $2\pi^*$ with an appropriate metal state. This model—commonly referred to as a Blyholder model, even though Blyholder originally applied a three-orbital picture to the π channel⁴⁷—neglects $1\pi-2\pi^*$ rehybridization. However, the importance of such effects for the adsorption of NO on nickel was already demonstrated a long time ago.²² Hence, a three-orbital model (usually illustrated for an allyl radical⁵⁰ or H_3 ⁵¹) which also takes into account the occupied 1π orbital of the adsorbate (as in Blyholder's original con-

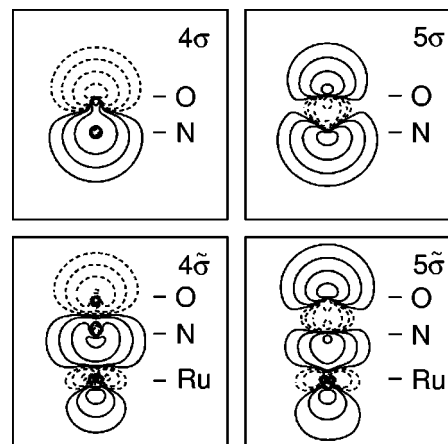


FIG. 6. Contour maps of the 4σ and 5σ orbitals of the free NO molecule and of the $4\tilde{\sigma}$ and $5\tilde{\sigma}$ cluster orbitals of the on-top adsorption model cluster Ru_{13}NO . The values of the contour lines are ± 0.32 , ± 0.10 , ± 0.032 and ± 0.010 a.u. The positions of the various atoms are indicated by horizontal bars.

TABLE IV. Fragment orbital analysis of various adsorption model clusters for the cluster π orbitals. Contributions of the NO reference orbitals (in percent) to the cluster orbitals. Contributions below 1% are not shown. From the manifold of $2\tilde{\pi}$ orbitals a high-energy ($2\tilde{\pi}_1$) and a low-energy ($2\tilde{\pi}_2$) representative are chosen. Energies in eV.

Orbital	Site	Energy	Free NO contributions	
			1π	$2\pi^*$
$1\tilde{\pi}$	top	12.95	92	2
	hcp	11.32	74	8
	fcc	11.51	81	5
$2\tilde{\pi}_1$	top	8.62	3	3
	hcp	7.72	8	2
	fcc	7.93	6	2
$2\tilde{\pi}_2$	top	4.42		1
	hcp	4.64	1	9
	fcc	4.75	1	7

cept) is much more appropriate. In fact, this ‘‘allyl model’’ has been applied successfully to the description of XES spectra of other dimers on metal surfaces before.¹¹ The key point of this allyl model is the formation of three entirely new orbitals of the adsorption complex as linear combinations of the 1π and the $2\pi^*$ MOs of NO (or alternatively, of the $2p_{x,y}$ from the two adsorbate atoms) and a suitable set of d frontier orbitals from the substrate. These three new orbitals are:

- a totally bonding orbital with equal phases and similar weights on all atoms,
- a nonbonding ‘‘lone pair’’ orbital mainly localized on the oxygen (and the metal), and
- a completely antibonding orbital with alternating phases between each pair of atoms.

They differ substantially from the orbitals originally obtained by Blyholder (for CO). This three-orbital interaction scheme is fully confirmed for NO adsorbed on Ru(001) by the present NO/Ru(001) model cluster calculations and will thus be applied in the following to explain the characteristic features of the XES spectra.

a. Analysis of the individual orbitals. All calculated spectra (Fig. 4) exhibit one isolated $1\tilde{\pi}$ peak and a further set of peaks which will be referred to as the ‘‘ $2\tilde{\pi}$ feature.’’ Similar to the interpretation of the σ channel, a fragment orbital analysis was applied to analyze the constitution of the relevant orbitals. The results are summarized in Table IV. The isolated $1\tilde{\pi}$ orbital which gives rise to the $1\tilde{\pi}$ signal in the XES spectra exhibits strong adsorbate character. It consists mainly of the NO 1π MO with minor contributions from the metal orbitals and the antibonding NO $2\pi^*$ orbital. The $2\pi^*$ admixture is in-phase on the nitrogen center and out-of-phase on the oxygen center; this leads to an interaction-induced polarization of the 1π orbital (which is more pronounced at the oxygen center than at the nitrogen center) towards the substrate, in accordance with the totally bonding orbital of the allyl model (see Fig. 7).

On the other hand, the manifold of orbitals which produces the $2\tilde{\pi}$ feature is dominated by the substrate while

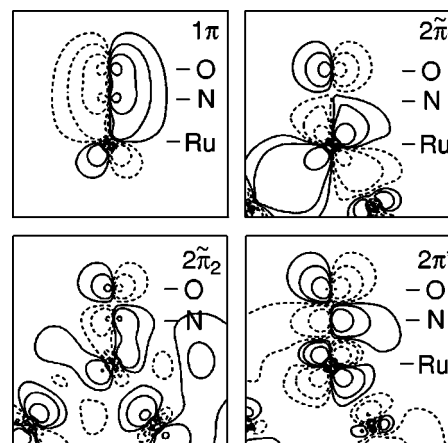


FIG. 7. Contour maps of selected orbitals of the on-top model cluster Ru_{13}NO shown in the (100) plane: The $1\tilde{\pi}$ orbital, one orbital of the high-energy end ($2\tilde{\pi}_1$), and one of the low-energy end ($2\tilde{\pi}_2$) of the back bonding manifold as well as a virtual orbital with a strong contribution of the molecular NO $2\tilde{\pi}$ orbital. The values of the contour lines are the same as in Fig. 5.

contributions of NO orbitals are rather small (Table IV). These contributions are derived from 1π and $2\pi^*$ admixtures of various weights. The 1π admixtures to the $2\tilde{\pi}$ orbital are antibonding, whereas the contribution from the $2\pi^*$ MO exhibits bonding character toward the substrate. As a result, the wave function amplitude on the nitrogen center is substantially reduced, but amplified on the oxygen center; thus, a lone pair orbital is formed which is the most characteristic feature of the allyl model discussed above. Because the NO contribution of this lone pair level is predominantly located on the oxygen center, the intensity of the $2\tilde{\pi}$ peak is much larger in the O-edge spectra than in the nitrogen spectra. The degree to which the wave function contributions in the lone pair orbital cancel each other strongly depends on the ratio of the 1π and $2\pi^*$ contributions. In general, the contribution of the NO 1π MO becomes less important with decreasing binding energy (i.e., with increasing orbital energy), whereas simultaneously the amount of the $2\pi^*$ MO admixture increases. This leads to a continuous change in the orbital character within the manifold of the $2\tilde{\pi}$ orbitals. At the high binding energy edge of the resonance, the nitrogen contribution almost vanishes and the lateral nodal plane of a representative $2\tilde{\pi}_1$ orbital nearly hits the nitrogen center (see Fig. 7). With decreasing binding energy, this nodal plane moves continuously toward the ‘‘outer’’ oxygen center, so that finally, at the low-energy edge of the resonance, it lies right between the two adsorbate atoms which is equivalent to an increase of the N $p_{x,y}$ contribution to the resonance. Nevertheless, the orbital still exhibits bonding character between the substrate and the nitrogen center. We were also able to identify the doubly antibonding orbital of the allyl model in our calculations. It exists as a virtual orbital in each of the cluster models (see Fig. 7 for the on-top site) roughly 1.5 eV above the Fermi level (Fig. 3) and thus does not contribute to x-ray emission.

b. Site specific differences. In principle, the orbital picture is equally valid for all three adsorption sites. However,

the fragment orbital analysis of the adsorption complexes reveals that, as a general trend, mixing between adsorbate and substrate orbitals is more distinct for NO adsorbed at the hollow sites. This can be rationalized by a simple geometric argument. Due to the absence of a metal atom directly below the NO molecule in the threefold sites, the NO species gets closer to the surface in comparison to the case for the on-top site. For this reason, and also because of the more suitable position of the nearest-neighbor Ru centers, the N $p_{x,y}$ orbitals overlap more strongly with the corresponding combinations of d orbitals on the three metal centers closest to the adsorbate. Admixtures of proper linear combinations of the more diffuse metal s -type orbitals are also involved at the hollow site, whereby rehybridization becomes very efficient. The enhanced interaction between substrate and adsorbate orbitals acts differently on the $1\tilde{\pi}$ and $2\tilde{\pi}$ cluster orbitals. In the NO-dominated $1\tilde{\pi}$ orbital, both the metal and the $2\pi^*$ contributions are larger than in the on-top cluster model; hence, the 1π admixture is smaller. In addition, admixture of the $2\pi^*$ orbital leads to a polarization of the $1\tilde{\pi}$ orbital from the oxygen to the nitrogen center. Thus, the nitrogen p population remains almost unchanged, whereas the oxygen p population decreases dramatically compared to on-top adsorption, in line with the XES intensity changes observed for the different adsorption sites.

On the other hand, in the substrate-dominated $2\tilde{\pi}$ orbitals, the enhanced adsorbate–substrate interaction results in a stronger adsorbate contribution. In fact, this reflects the stronger back donation at the hollow sites already discussed in Sec. IV A. As a consequence, the $2\tilde{\pi}$ peak exhibits a higher intensity in the hollow-site spectra than in the spectra for the on-top site. However, as is evident from Figs. 4(a) and 4(b), the intensity of the N-edge signal does not increase by the same amount as the O-edge signal. This particular finding is due to the stronger admixtures of the 1π orbitals to the lone pair orbitals $2\tilde{\pi}$ of the hollow-site adsorption complex which causes a polarization of the lone pair orbital from the nitrogen to the oxygen atom. Thus, the enhanced back donation encountered for hollow-site adsorption complexes (compared to on-top adsorption) only shows up in an increase of the $2\tilde{\pi}$ intensity of the O-edge spectra. This correlation between back donation and intensity of the $2\tilde{\pi}$ signal at the O-edge also holds for a comparison of the two hollow sites. The intensity ratio of the $2\tilde{\pi}$ and $1\tilde{\pi}$ signals is larger at the hcp site than at the fcc site [Fig. 5(c)], in line with the slightly weaker back donation at the latter site (Table I).

To continue the discussion at the end of Sec. IV A, there is no straightforward coherence between the strength of the back donation and the elongation of the NO bond length. The lone pair-like $2\tilde{\pi}$ orbitals of the adsorbate complex actually exhibit a lower NO antibonding character than the molecular $2\pi^*$ orbital. Thus, the slightly shorter bond length of NO adsorbed at the on-top site (compared to the gas phase) is not at variance with the back donation found in the present calculations.

c. Comparison with the experimental spectra. Experimentally, only two signals are observed in the π channel [see

Figs. 5(a), 5(b)]. The internal structure of the $2\tilde{\pi}$ feature discernible in the transition-weighted DOS curves is not resolved in the recorded XES spectra. On the one hand, this may be related to the broadening of the x-ray emission signal and to the limited resolution of the experiment (including lifetime effects). On the other hand, details of the $2\tilde{\pi}$ feature may very well be a consequence of the finite cluster model adopted here which would change into continuous resonance-like features in case of a semi-infinite substrate model. To account for the experimental linewidths and to facilitate comparison with the experiment, a larger broadening factor of 1.2 eV has been used in the symmetry-resolved projected simulations of Fig. 6(c). Thereby, the $2\tilde{\pi}$ manifold discernible in Figs. 4(a)–4(c) evolves into a single broader and higher peak, similar to that in the experimental data. We do not expect that such broadened spectra will show any significant cluster size dependences.

The general agreement between the experimental spectra and the simulated spectra based on 1.2 eV broadening is remarkable, i.e., all salient features of the experimental spectra including site-specific differences are reproduced: For all sites, the intensity of the oxygen $2\tilde{\pi}$ signal is much higher compared to the nitrogen signal. The energy of the $2\tilde{\pi}$ feature in the O-edge spectrum is shifted relative to its position in the N-edge spectrum due to the continuous change of orbital character in this resonance (see subsection *a*). Switching from the on-top to the hollow sites leads to a pronounced increase of the $2\tilde{\pi}$ signal. In the oxygen spectra, this is accompanied by a substantial decrease of the $1\tilde{\pi}$ signal, which finally results in the interchange of the relative intensities of the O $1\tilde{\pi}$ and $2\tilde{\pi}$ signals.

C. XES energies

With regard to the energetics of the emission, it is worth mentioning that the ordering of the signals in the simulated and the experimental spectra is the same. This is insofar remarkable as the ordering of the $5\tilde{\sigma}$ and $1\tilde{\pi}$ signal is inverted in comparison to the 5σ and 1π MOs of NO in the gas phase. Because of the considerable broadening of some of the peaks in the measured spectra, a meaningful quantitative comparison of the experimental and theoretical results is only possible for the energy differences between the $4\tilde{\sigma}$ and $5\tilde{\sigma}$, the $5\tilde{\sigma}$ and $1\tilde{\pi}$, as well as the $1\tilde{\pi}$ and $2\tilde{\pi}$, signals (Table V). The general trends are roughly reproduced, but overall agreement is poor. This is most probably related to the frozen ground-state approximation adopted here, i.e., to the deficiencies of Kohn–Sham one-particle energies as a base for an accurate description of *valence* ionization energies. This problem is not specific to XES; it would also have been encountered in the simulation of ultraviolet photoemission spectra (UPS) of NO/Ru(001). Actually, approaches to improve valence ionization energies within the Kohn–Sham methodology are known, and have already been applied in the framework of simulations of XES spectra.¹³ Different Kohn–Sham Hamiltonians for each valence hole state may be useful for improving the valence ionization energies (e.g., Slater’s transition state rule⁵²), but cannot be

TABLE V. Comparison between calculated and experimental binding energy differences ΔE (in eV). The theoretical values are extracted from spectra with a broadening of 1.2 eV [Fig. 6(c)]. The calculated hollow-site data refer to the hcp model. Unless stated differently, symmetry splitting due to lateral interaction is not resolved experimentally.

	Calc.		Expt.	
	XES(N)	XES(O)	XES(N)	XES(O)
On-top site				
$\Delta E(5\tilde{\sigma}-4\tilde{\sigma})$	3.9	3.9	5.2	4.8
$\Delta E(1\tilde{\pi}-5\tilde{\sigma})$	0.5	0.5	1.7	1.9
$\Delta E(2\tilde{\pi}-1\tilde{\pi})$	7.3	6.1	5.4	3.1
Hollow site				
$\Delta E(5\tilde{\sigma}-4\tilde{\sigma})$	5.6	5.6	6.4	5.3
$\Delta E(1\tilde{\pi}-5\tilde{\sigma})$	0.5	0.5	1.6,0.5 ^a	1.6
$\Delta \epsilon(2\tilde{\pi}-1\tilde{\pi})$	6.7	5.4	5.1,6.2 ^a	3.1

^aSplit due to symmetry breaking in $(2 \times 1)\text{-NO}+\text{O}/\text{Ru}(001)$ (Ref. 17).

used for the determination of transition probabilities in a straightforward manner because of the nonorthogonality of the involved sets of one-particle wave functions. Attempts to obtain better results for the energetics by using an exchange-correlation functional with improved asymptotics⁵³ failed; the relative positions of the valence Kohn–Sham one-particle energies could not be significantly improved.

It has been argued in Sec. III B that the energetics of the XES process should coincide with the energetics of direct photoemission. Indeed, the equality of UPS and XES quasi-particle energies is not always corroborated experimentally.¹⁷ Thus, one may argue that such deviations may also contribute to the rather poor agreement of experimental and calculated XES energies. However, inspection of UPS data recently recorded for NO on Ru(001)¹⁷ reveals that this line of reasoning does not apply to NO/Ru(001).

V. SUMMARY

We have presented a quantum chemical analysis of the x-ray emission spectra of NO adsorbed on Ru(001). Symmetry resolved densities of states, weighted by the transition probabilities, were employed to simulate the XES spectra. Evaluation of the dipole transition matrix elements within the frozen ground-state approximation proved satisfactory for this purpose. The entire set of experimentally recorded x-ray emission spectra of NO/Ru(001) is reproduced properly, including the characteristic distinctions between N- and O-edge spectra as well as all adsorption site-specific differences.

Based on the DF model cluster calculations and supported by the experimental population analysis provided by the XES data, a consistent picture of the chemical bond was derived. The adsorption of NO on the Ru(001) surface is accompanied by a significant electron charge transfer from NO to the substrate in the σ channel and a reverse charge flow in the π channel for all adsorption sites considered here (Blyholder model). However, in contrast to the common variant of the classical Blyholder model, interaction in both σ and π channels is best described by a three-orbital inter-

action pattern, which for the π channel is very similar to that of an allyl radical (allyl model). In addition, π back donation is not simply related to an increase of the NO $2\pi^*$ orbital occupation. Rather, it is manifested as a broad manifold of metal-dominated orbitals with small contributions from both, the NO $2\pi^*$ and the NO 1π orbitals. The orbitals which give rise to the $2\tilde{\pi}$ signal actually exhibit lone pair character (with little or no contribution at the N center), while the antibonding NO π^* orbital is mainly subsumed in a fully antibonding unoccupied orbital above the Fermi level. Similarly, upon adsorption the NO σ orbitals strongly rehybridize such that the 4σ orbital is polarized toward the nitrogen center, whereas the 5σ orbital is polarized in the opposite direction. This overall bonding mechanism is equally valid for both the on-top and hollow-site species, the only difference being that adsorbate and substrate π orbitals mix in a more pronounced fashion in the case of hollow-site adsorption.

Despite the frozen ground-state approximation utilized here, the achieved agreement between the theoretical and experimentally derived spectra is remarkable. Obviously, neglecting relaxation effects in both initial and final states does not harm the calculated transition intensities in a serious fashion. This finding seems to be rather general, since results of similar quality have been obtained for other adsorption systems as well.^{11–13}

ACKNOWLEDGMENTS

This work was supported by the Deutsche Forschungsgemeinschaft via SFB No. 338 and by the Fonds der Chemischen Industrie.

- R. A. Matison and R. C. Ehlert, J. Chem. Phys. **48**, 5465 (1968).
- R. A. Matison and R. C. Ehlert, J. Chem. Phys. **48**, 5471 (1968).
- R. Manne, J. Chem. Phys. **52**, 5733 (1970).
- A. Meisel, G. Leonhardt, and R. Szargan, *Röntgenspektren und Chemische Bindung* (Geest&Portig, Leipzig, 1977).
- H. Tillborg, A. Nilsson, T. Wiell, N. Wassdahl, N. Mårtensson, and J. Nordgren, Phys. Rev. B **47**, 16464 (1993).
- A. Nilsson, P. Bennich, T. Wiell, N. Wassdahl, N. Mårtensson, J. Nordgren, O. Björneholm, and J. Stöhr, Phys. Rev. B **51**, 10244 (1995).
- A. Nilsson, N. Wassdahl, M. Weinelt, O. Karis, T. Wiell, P. Bennich, J. Hasselström, A. Föhlisch, J. Stöhr, and M. Samant, Appl. Phys. A: Mater. Sci. Process. **65a**, 147 (1997).
- M. Weinelt, N. Wassdahl, T. Wiell, O. Karis, J. Hasselström, P. Bennich, A. Nilsson, J. Stöhr, and M. Samant, Phys. Rev. B **58**, 7351 (1998).
- L. Triguero, Y. Luo, L. G. M. Pettersson, H. Ågren, P. Väterlein, M. Weinelt, A. Föhlisch, J. Hasselström, O. Karis, and A. Nilsson, Phys. Rev. B **59**, 5189 (1999).
- A. Nilsson, M. Weinelt, T. Wiell, P. Bennich, O. Karis, N. Wassdahl, J. Stöhr, and M. Samant, Phys. Rev. Lett. **78**, 2847 (1997).
- P. Bennich, T. Wiell, O. Karis, M. Weinelt, N. Wassdahl, A. Nilsson, M. Nyberg, L. G. M. Pettersson, J. Stöhr, and M. Samant, Phys. Rev. B **57**, 9274 (1998).
- V. Carravetta, L. G. M. Pettersson, O. Vahtras, and H. Ågren, Surf. Sci. **369**, 146 (1996).
- L. Triguero, L. G. M. Pettersson, and H. Ågren, J. Phys. Chem. A **102**, 10599 (1998).
- L. Triguero and L. G. M. Pettersson, Surf. Sci. **398**, 70 (1998).
- L. Triguero, L. G. M. Pettersson, and H. Ågren, Phys. Rev. B **58**, 8097 (1998).
- L. G. M. Pettersson, H. Ågren, Y. Luo, and L. Triguero, Surf. Sci. **408**, 1 (1998).
- M. Stichler, C. Keller, C. Heske, M. Staufer, U. Birkenheuer, N. Rösch, W. Wurth, and D. Menzel (unpublished).

- ¹⁸K. M. Neyman, K. L. Kostov, P. Jakob, N. Rösch, and D. Menzel, *J. Chem. Phys.* **100**, 2310 (1994).
- ¹⁹M. Stichler and D. Menzel, *Surf. Sci.* **391**, 47 (1997).
- ²⁰M. Stichler and D. Menzel, *Surf. Sci.* **419**, 272 (1999).
- ²¹A. Schichl, D. Menzel, and N. Rösch, *Chem. Phys.* **65**, 225 (1982).
- ²²A. Schichl and N. Rösch, *Surf. Sci.* **137**, 261 (1984).
- ²³T. Wiell, Ph.D. thesis, Uppsala University, 1995.
- ²⁴P. Bennich, Ph.D. thesis, Uppsala University, 1996.
- ²⁵O. Karis, Ph.D. thesis, Uppsala University, 1997.
- ²⁶P. Baltzer, J.-O. Forsell, A. Nilsson, B. Wannberg, A. Stenborg, N. Mårtensson, and P. A. Bruhwiler, *J. Electron Spectrosc. Relat. Phenom.* **70**, 117 (1994).
- ²⁷J. Stöhr, *NEXAFS* (Springer Series in Surface Sciences 6, New York, 1992).
- ²⁸J. Nordgren and R. Nyholm, *Nucl. Instrum. Methods Phys. Res. A* **246**, 242 (1986).
- ²⁹J. Nordgren, G. Bray, S. Cramm, R. Nyholm, J.-E. Rubensson, and N. Wassdahl, *Rev. Sci. Instrum.* **60**, 1690 (1989).
- ³⁰PARAGAUSS 1.9, T. Belling, T. Grauschopf, S. Krüger, F. Nörtemann, M. Staufer, M. Mayer, V. A. Nasluzov, U. Birkenheuer, and N. Rösch, Technische Universität München, 1998.
- ³¹T. Belling, T. Grauschopf, S. Krüger, M. Mayer, F. Nörtemann, M. Staufer, C. Zenger, and N. Rösch, "Quantum Chemistry on Parallel Computers: Concepts and Results of a Density Functional Method," in *Proceedings of the First International FORTWIHR Conference 1998: High Performance Scientific and Engineering Computing*, edited by F. Durst and C. Zenger, *Lecture Notes in Computational Science and Engineering* (Springer, Heidelberg, 1999), p. 439.
- ³²B. I. Dunlap and N. Rösch, *Adv. Quantum Chem.* **21**, 317 (1990).
- ³³N. Rösch, in *Cluster Models for Surface and Bulk Phenomena, NATO ASI Series B*, edited by G. Pacchioni, P. S. Bagus, and F. Parmigiani (Plenum, New York, 1992), p. 251.
- ³⁴S. Huzinaga, *J. Chem. Phys.* **66**, 4245 (1977).
- ³⁵R. Poirier, R. Kari, and I. G. Csizmadia, *Handbook of Gaussian Basis Sets. A Compendium for Ab Initio Molecular Orbital Calculations* (Elsevier, Amsterdam, 1985).
- ³⁶F. B. van Duijnefeldt, IBM Research Report RJ945 (1971).
- ³⁷*Gaussian Basis Sets*, edited by S. Huzinaga (Elsevier, Amsterdam, 1984).
- ³⁸R. C. Raffanetti, *J. Chem. Phys.* **58**, 4452 (1973).
- ³⁹S. H. Vosko, L. Wilk, and M. Nusair, *Can. J. Phys.* **58**, 1200 (1980).
- ⁴⁰J. P. Perdew, J. A. Chevary, S. H. Vosko, K. A. Jackson, M. R. Pederson, D. J. Singh, and C. Fiolhais, *Phys. Rev. B* **46**, 6671 (1992).
- ⁴¹W. Wurth, C. Schneider, R. Treichler, E. Umbach, and D. Menzel, *Phys. Rev. B* **35**, 7741 (1987).
- ⁴²A. Sandell, O. Björneholm, A. Nilsson, B. Hernäs, J. N. Andersen, and N. Mårtensson, *Phys. Rev. B* **49**, 10136 (1987).
- ⁴³M. Weinelt, W. Huber, P. Zebisch, H.-P. Steinrück, P. Ulbricht, U. Birkenheuer, J. C. Boettger, and N. Rösch, *Surf. Sci.* **345**, 331 (1996).
- ⁴⁴U. Birkenheuer, U. Gutdeutsch, N. Rösch, A. Fink, S. Gokhale, D. Menzel, P. Trischberger, and W. Widdra, *J. Chem. Phys.* **108**, 9868 (1998).
- ⁴⁵U. Birkenheuer, U. Gutdeutsch, and N. Rösch, *Surf. Sci.* **409**, 213 (1998).
- ⁴⁶H. Koschel, G. Held, P. Trischberger, W. Widdra, U. Birkenheuer, and H.-P. Steinrück, *Appl. Surf. Sci.* **142**, 18 (1999).
- ⁴⁷G. Blyholder, *J. Phys. Chem.* **68**, 2772 (1964).
- ⁴⁸P. Jakob, M. Stichler, and D. Menzel, *Surf. Sci. Lett.* **370**, L185 (1997).
- ⁴⁹P. Jakob, S. Kulkarni, E. Umbach, and D. Menzel, *Surf. Sci.* **99**, 489 (1980).
- ⁵⁰D. L. DuBois and R. Hoffmann, *Nouv. J. Chim.* **1**, 479 (1977).
- ⁵¹T. A. Albright, J. K. Burdett, and M.-H. Whangbo, *Orbital Interactions in Chemistry* (Wiley, New York, 1985), pp. 36–38.
- ⁵²J. C. Slater, *The Self-Consistent Field for Atoms and Molecules* (McGraw-Hill, New York, 1974).
- ⁵³R. van Leeuwen and E. J. Baerends, *Phys. Rev. A* **49**, 2421 (1994).